Proceedings of the IASS 2024 Symposium
Redefining the Art of Structural Design
August 26-30, 2024, Zurich Switzerland
Philippe Block, Giulia Boller, Catherine DeWolf,
Jacqueline Pauli, Walter Kaufmann (eds.)

Research on Seismic Performance of Super-Large Span Mega-latticed Structures Retrofitted with GFRP

Bo Huang[a,b], Xudong Zhi[a,b,*]

*School of Civil Engineering, Harbin Institute of Technology, Harbin, 150090, China
No.73 Huanghe Road, Harbin, China
zhixudong@hit.edu.cn

[a] Key Lab of Structures Dynamic Behavior and Control of the Ministry of Education, Harbin Institute of Technology, Harbin, 150090, China
[b] Key Lab of Smart Prevention and Mitigation of Civil Engineering Disasters of the Ministry of Industry and Information, Technology, Harbin Institute of Technology, Harbin, 150090, China

Abstract

To mitigate the significant impact of self-weight and enhance the seismic performance of Super-Large Span Mega-latticed Structures(SSMS), the lightweight, high-strength, and corrosion-resistant glass fiber reinforced polymer (GFRP) was adopted to retrofit the SSMS components. Initially based on the safety factor slightly exceeding 2, the three-dimensional grid dome-type SSMS with an 800m span and a three-type rise-span ratio(1/5 to 1/10) was designed and defined as the basic condition. Subsequently, the GFRP volume ratio(KF) from 30% to 80% was adopted to retrofit the components in the basic condition, the WQJ equivalent formula was adopted simplified the composite component, while an equal section size steel structure served as the control group. An analysis of the impact of the GFRP volume ratio on enhancing the static stability and seismic peformance of the structure was conducted, the seismic damage states and the corresponding loss efficiency of SSMS were defined, and the economic aspects of the GFRP-retrofitted structure under equal safety factors were discussed. The results demonstrate that structure density can be reduced by 60% by increasing KF; GFRP retrofitted structures have better static stability than the control group when KF about 58%, and the improvement is greater at low rise-span ratios. The GFRP retrofitted structure has better seismic performance when KF>50%. Hence, KF=50%~60% was more suitable for the GFRP retrofitted SSMS.

Keywords: Super-large span, Mega-latticed structures, Seismic performance, GFRP, Static stability

1. Introduction

To enhance the urban resilience during or after natural disasters such as hurricanes, heatwaves, earthquakes, and hazes, and to achieve urban construction in extreme environments, the idea of ‘kilometer-scale urban domes’ emerged as the times require[1-2]. Various hybrid structural forms, such as suspen-dome structures[3, 4], pretensioned spherical reticulated mega-structures, giant grid suspend-domes[5], the cylindrical reticulated mega-structure[6] and the Kiewitt type mega-latticed structure was evoluted[7], have been successively applied to meet the demands for the structural force and stability of supe-large span structures. However, in the studies on seismic performance[8], static performance, and stability[9-11] of SSMS, it is found that the structural weight has a significant impact on the overall performance of SSMS, which has become a problem to be solved in the super-large span structure.

FRP-metal composite component has the characteristics of lightweight, high strength, and corrosion resistance. Various forms of composite component have been utilized in structural components such as

concrete beams and columns[12, 13], reinforced concrete shear walls[14], and architectural circular steel pipes[15] in the field of civil engineering, and showed the characteristics of improving the overall strength and significantly reducing the self-weight. In addition, the mechanical performance of composite component under loading conditions such as bending, shear, impact, axial compression, and hysteresis has received widespread attention. There has been a particular focus on discussing the effects of parameters such as diameter-to-thickness ratio, fiber orientation, and number of fiber layers on the mechanical performance of composite component[16]. Various performance prediction formulas for composite members have been proposed, laying a solid research foundation. However, there is relatively limited research on the mechanical performance of overall structural systems constructed using composite components. Applications in the field of super-large span spatial structures are still lacking. Therefore, this paper conducts ultimate stress design on three-dimensional grid dome-type SSMS with spans of 800m and rise-span ratios of 1/5, 1/7, and 1/10, and obtains the basic conditions where the stable bearing capacity meets the requirement of twice the safety factor. On this basis, reinforcement was carried out using GFRP with KF values of 30%, 60%, and 80%, an architectural circular steel pipe component structure with equal cross-sectional dimensions was used as the control group, the effects of GFRP volume ratio on the structural static performance, stability, and seismic performance was analyzed. Taking into account economic factors, a reasonable range of KF values for GFRP-reinforced SSMS is proposed, laying the foundation for further research on SSMS.

2. FE model of super-large span mega-latticed structures

2.1. Basic condition and FE model

The structure of the three-dimensional grid dome-type SSMS, with spans of 800m and rise-span ratios of 1/5, 1/7, and 1/10, established using traditional architectural circular steel pipes, serves as the basic condition. The structure has a radial grids number of 5 and a circumferential grids number of 6. The dimensions of the mega-grid truss are 5.2511m in height and width, with a segment length of 8.1683m. Using the method proposed by An[17], a finite element model of a three-dimensional grid dome-type SSMS was established in ANSYS software. The model was created sequentially by generating single-layer reticulated shell structures, various conical nodes, and different regional truss members, as shown in Figure 1a.

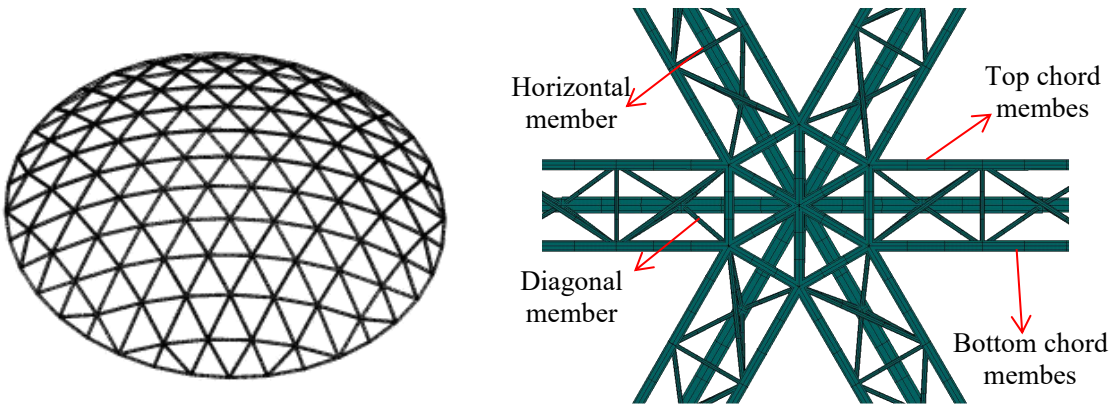

a) elevation view b) Truss of mega-latticed stucture

Figure 1: Finite element model for three-dimensional grid dome-type mega-latticed structure

The members are simulated using Beam188 beam elements, and the material model adopts the ideal elastic-plastic constitutive model of Q420 steel. The specific parameters are as follows: yield strength of 420 MPa, elastic modulus of 211 GPa, and Poisson's ratio of 0.3. The connection type of each member is rigid, and the boundary conditions are three-way simply supported around the lower chord. Live loads and dead loads of 0.5 kN/m2 and 1.4 kN/m2, respectively were chosen. The gravity load is directly applied to the members of the model, while the dead load and live load are applied uniformly to the upper chord nodes of the model. The structural viscous damping ratio is set according to the

requirements of the "Technical Specifications for Space frame Structures" at 0.02, and initial geometric imperfections of L/300 are considered. Subsequently, stress design and section optimization are conducted for each basic condition to ensure that the structural stable bearing capacity meets the requirement of twice the safety factor. The safety factor values for each basic condition are listed in Table 2. The naming convention for basic conditions, taking "D80005" as an example, follows this pattern: "D" represents the grid dome-type SSMS, "800" indicates the span, and "05" represents the reciprocal of the rise-span ratio.

2.2. GFRP composite structure design and modeling

Compared to architectural circular steel pipes, composite pipes stand out primarily due to their lightweight, high strength, and excellent environmental durability. This is particularly important in large-span spatial structures where self-weight is a primary load. Therefore, three different GFRP volume ratios (KF) of 30%, 60%, and 80% were selected to reinforce all members of the basic conditions, referred to as the GFRP group conditions. The naming convention adds "K" (KF) followed by the corresponding KF value to the name of the basic condition. For example, "D80005K30" denotes the D80005 structure reinforced by GFRP of KF = 30%. Simultaneously, a traditional architectural circular steel pipe structure with the same cross-sectional dimensions as the members in the GFRP group conditions was used as a control group. This allowed for a comparative analysis of the enhancement effects of GFRP on the structural performance. The control group is denoted by adding "C" (Control) followed by the corresponding KF value to the name of the basic condition. For example, "D80005C30" signifies the control group condition for "D80005K30".

The modeling process for both the GFRP group and the control group conditions is similar to that of the basic conditions. However, the composite structure of GFRP group conditions modeling by solid elements is complex and computationally time-consuming.Therefore, after determining parameters such as fiber layer thickness (t_F) and outer diameter (D_F) based on the dimensions of the basic condition members (outer diameter D, thickness t), as well as the KF value, the composite components in the structure were simplified using the WQJ equivalent formula[18]. This simplified the fiber layer and the architectural circular steel pipe into an equivalent circular steel pipe component with equivalent outer diameter (D_{eq}), equivalent thickness (t_{eq}), and equivalent density (ρ_{eq}), other material parameters being the same as Q420 steel. The specific calculation method is shown in Eqs. (1) and (3). Then, modeling was performed using the parameters of the equivalent circular steel pipe. The control group adopts architectural circular steel pipes with the same cross-sectional dimensions as the GFRP composite pipes (outer diameter D_F, thickness $t + t_F$) for modeling.

$$\begin{cases} I_{eq} = I_S + \Delta_2 \cdot I_F \\ t_{eq} = 0.5\left[\dfrac{64\left(I_{eq} - I_S\right)}{\pi} + D^4\right]^{1/4} - 0.5D \\ D_{eq} = D + 2t_{eq} \end{cases} \tag{1}$$

In the equation, I_{eq} represents the equivalent moment of inertia, while I_s and I_F represent the moments of inertia of the architectural circular steel pipe and the fiber layer, respectively; D represents the outer diameter of the architectural circular steel pipe; Δ_2 is the GFRP material participation coefficient, as shown in Eq(2).

$$\begin{cases} E_{eq}^{\ x} = 1/\left(1/E_1^c \cdot \cos^4\theta + \left(1/G_{12} - 2\nu_{12}/E_1^c\right) \cdot \sin^2\theta \cdot \cos^2\theta + 1/E_2^c \cdot \sin^4\theta\right) \\ \Delta_2 = \dfrac{E_{eq}^{\ x} \cdot I_F + E_{eq}^{\ y} \cdot I_F \cdot \nu_{12}}{E_{eq}^{\ x} \cdot I_F + E_{eq}^{\ y} \cdot I_F \cdot \nu_{12} + E_S \cdot I_S} \\ E_{eq}^{\ y} = 1/\left(1/E_1^t \cdot \sin^4\theta + \left(1/G_{12} - 2\nu_{12}/E_1^t\right) \cdot \sin^2\theta \cdot \cos^2\theta + 1/E_2^t \cdot \cos^4\theta\right) \end{cases} \tag{2}$$

In the equation, E_{eq}^{x} represents the equivalent axial compression modulus of GFRP (GPa), and E_{eq}^{y} represents the equivalent circumferential tensile modulus of GFRP (GPa). E_{1c}, E_{1t}, G_{12}, E_{2t}, E_{2c}, v_{12} are specific parameters of GFRP materials, as shown in Table 1.

$$\rho_{eq} = \frac{m_F + m_S}{V_F + V_S} = K_F \rho_F + (1 - K_F)\rho_S \tag{3}$$

In the equation, m_F and m_s represent the mass of the architectural circular steel pipe and the fiber layer, respectively; V_F and V_s represent their respective volumes, and ρ_F and ρ_s represent their densities.

Table 1: GFRP material parameter

Parameter	Value
Modulus/GPa	E_1^t=41.29; E_1^c=42.37; E_2^t=E_3^t=4.21; E_2^c=E_3^c=11.7; G_{12}=G_{13}=G_{23}=3.16
Poisson's ratio	v_{12}=v_{13}=0.31; v_{23}=0.42

3. Static stability analysis of fiber-reinforced SSMS

3.1. Buckling mode analysis

By conducting linear stability analyses on basic conditions of different rise-span ratio of three-dimensional grid dome-type SSMS, the lowest order buckling modes of the two structures were obtained, as shown in Figure 2. It can be observed that the buckling modes for rise-span ratios of 1/7 and 1/10 are essentially identical and exhibit significant similarity to those for thhe rise-span ratio of 1/5. These buckling modes typically manifest as the sagging downward of nodes at the intersections of the trusses at the third ring, Causing adjacent trusses near the bottom protruding outward, resulting in a wavy deformation pattern across symmetrical regions of the structure, and most trusses lose their load-bearing capacity due to excessive bending deformation of the spherical surface leading to buckling failure. Compared to the rise-span ratio of 1/5, the difference lies in the fact that the more widely sagging range extends from the second to the fourth ring for rise-span ratios of 1/7 and 1/10, and the more significant outward protrusion in the first ring area relative to the 5-6 ring area. This is because, with a decrease in rise-span ratio, the effect of gravity becomes more pronounced. In the analysis of the GFRP group conditions, it was found that increasing KF did not significantly alter the buckling modes, indicating a minor influence of fiber reinforcement on the buckling modes of the structure.

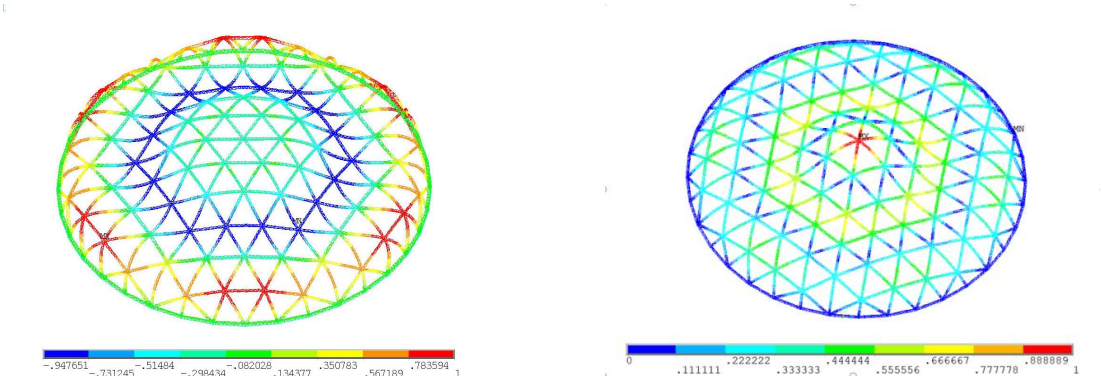

a) Buckling mode of 1/5 rise-span ratio structure b) Buckling mode of 1/7, 1/10 rise-span ratio structure

Figure 2: Buckling mode of three-dimensional grid dome-type SSMS

3.2. Static stability analysis

The results of static stability analysis for different conditions are listed in Table 2. From the table, it can be seen that the improvement in overall structural stability with KF = 30% is approximately 10%, indicating relatively poor enhancement. However, with KF values at 60%, the improvement in

structural stability is significantly more pronounced, reaching around 60%. Furthermore, with KF = 80%, the enhancement can even exceed 300% compared to the basic structure.

Table 2: Stability analysis results of three-dimensional grid mega-lattice structure

GFRP Group	Stability Capacity (kN/m^2)	Safety Factor	Improvement Ratio (%)	Control Group	Stability Capacity (kN/m^2)	Safety Factor
D80005	4.43	2.33	0.00	-	4.43	2.33
D80005_K30	4.96	2.61	12.02	D80005_C30	6.54	3.44
D80005_K60	7.71	4.06	74.25	D80005_C60	11.21	5.90
D80005_K80	18.81	9.90	324.89	D80005_C80	15.00	7.89
D80007	4.38	2.31	0.00	-	4.38	2.31
D80007_K30	4.94	2.60	12.70	D80007_C30	6.46	3.40
D80007_K60	7.49	3.94	70.78	D80007_C60	11.04	5.81
D80007_K80	18.68	9.83	326.09	D80007_C80	14.14	7.44
D80010	4.39	2.31	0.00	-	4.39	2.31
D80010_K30	5.58	2.94	27.14	D80010_C30	6.73	3.54
D80010_K60	8.55	4.50	94.72	D80010_C60	11.36	5.98
D80010_K80	21.11	11.11	380.95	D80010_C80	15.81	8.32

Figure 3 shows that when KF is above 65%, the safety factor of the GFRP group significantly surpasses that of the control group. However, for KF values between 0 and 60%, the GFRP group performs slightly worse than the control group at different rise-span ratios. This is due to the smaller thickness of GFRP at lower KF values, resulting in a significant performance gap between the fiber layer and the steel pipe and thus poorer compatibility. Consequently, the enhancement effect is not ideal. As KF values increase, the thickness of the fiber layer increases, leading to improved compatibility with the steel pipe. This aligns with Wu's research indicating that composite components tend to perform better when the fiber layer thickness relatively exceeds that of the steel pipe.

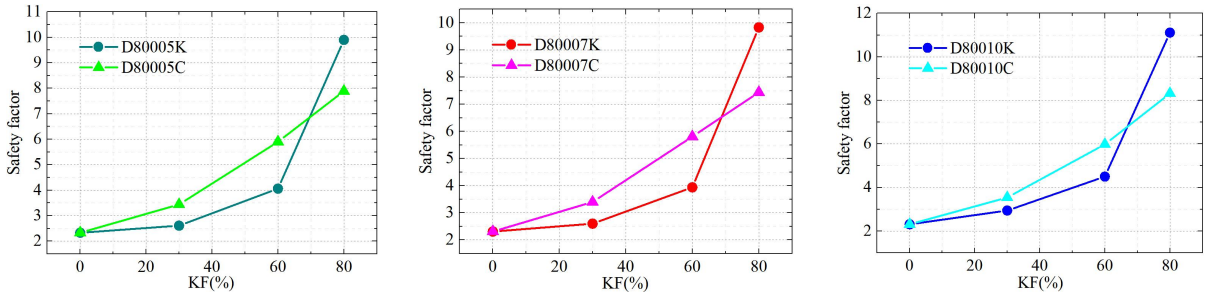

a) 1/5 rise-span ratio b) 1/7 rise-span ratio c) 1/10 rise-span ratio

Figure 3: Comparative analysis of fiber reinforcement effects on structural stability

Comparing different rise-span ratios conditions, it's observed that as the rise-span ratio decreases, the difference between the GFRP-reinforced and control groups decreases when KF is less than 65%. Moreover, for rise-span ratios of 1/5, 1/7, and 1/10, the critical KF values where both groups have equal safety factors are 64.8%, 63.7%, and 62.6% respectively, also showing a decreasing trend. At KF = 80%, the enhancement effect of GFRP under the 1/10 rise-span ratio condition is notably better than under the 1/5 and 1/7 conditions. This indicates that the effect of self-weight is more significant in structures with smaller rise-span ratios, especially in kilometer-scale SSMS. The impact of self-weight is more pronounced in structures with smaller rise-span ratios, particularly in kilometer-scale SSMS.

3.3. Static performance analysis

The static performance analysis of GFRP-reinforced structures primarily focuses on analyzing two aspects: peak stress and maximum nodal displacement of the structure. The comparative analysis with the control group is presented in Figure 4, reveals a trend in changes similar to the stability analysis. As the rise-span ratio decreases, the amplitude of the difference from the control group gradually diminishes. At a rise-span ratio of 1/10, there is a nearly overlapping trend. The KF_{CV} (KF critical values) for peak stress occur at 57.6%, 46.9%, and 37.8% for rise-span ratios of 1/5, 1/7, and 1/10, respectively. Similarly, the KF_{CV} for maximum node displacement occur at 49.8%, 48.7%, and 39.2% for the same rise-span ratios. When KF is greater than 60%, the static performance of the GFRP group significantly surpasses that of the control group, with the most noticeable improvement observed in the 1/10 rise-span ratio condition.

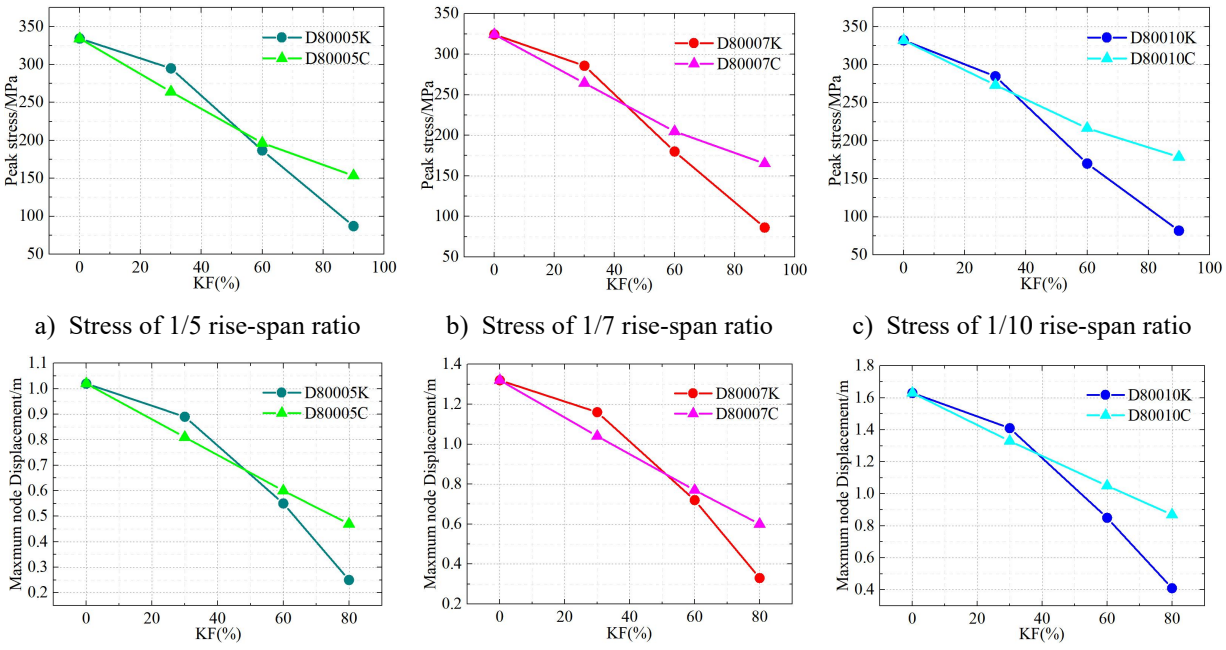

a) Stress of 1/5 rise-span ratio
b) Stress of 1/7 rise-span ratio
c) Stress of 1/10 rise-span ratio
d) Displacement of 1/5 rise-span ratio
e) Displacement of 1/7 rise-span ratio
f) Displacement of 1/10 rise-span ratio

Figure 4: Comparative analysis of fiber reinforcement effects on structural static performance

This is because larger rise-span ratios create an "arch" load-bearing state, while smaller rise-span ratios result in a "flat shell" load-bearing state similar to a "beam". Structures with larger spans and smaller rise-span ratios are more affected by self-weight, fiber composite components effectively reduce this effect. Furthermore, compared to structures with smaller spans and larger rise-span ratios, such structures select larger cross-sectional dimensions, the fiber layer thickness is relatively larger at the same KF value, hence the enhancement effect on the load-bearing capacity of the members is stronger, leading to a more significant improvement in the static performance of GFRP in structures with larger spans and smaller rise-span ratios.

4. Seismic performance analysis of fiber-reinforced SSMS

4.1. Damage state of SMSS

Due to the fact that the model of SSMS is formed by generating cone nodes and truss members through conventional reticulated shell structures, its stress and failure characteristics are similar, hence a method similar to that used for reticulated shell structures was adopted to classify the seismic damage state(DS) as shown in Table 3. The classification of damage states mainly depends on the extent of damage and yielding of the members and the overall stiffness of the structure. Therefore, the assessment primarily focuses on: 1) the proportion of yielding members: The number of yielding

points in each beam element with 8 integration points; 2) Maximum node displacement; 3) the average structural plastic strain: representing the depth of structural plastic development. The critical values between different damage states are represented using the Limit State (LS). The threshold between Insignificant and Minor damage is defined as LS1, and so on, theSSMS includes four limit states.

Table 3: Definition and description of the performance levels of SSMS

DS	Response	Criteria	Repair measures
Insignificant	Members are intact	Members in elastic state	Normal use
Minor	Minor yielding members, limited plastic deformation.	No 8P plasticized members	Slight repair
Moderate	Most members yield, but haven't fractured; No significant change in structural stiffness.	Structural stiffness and strength severely weakened; Partial members failure	Reinforcement required for continued use.
Severe	Significant decrease in structural stiffness; Some members fractured	Before structural failure	Structural repair required, partial dismantling
Collapse	Collapsed	After structural failure	Demolition required

4.2. Seismic performance analysis

To investigate the enhancement effect of GFRP on the seismic performance of the structure, IIncremental Dynamic Analysis (IDA) was conducted for each condition using tri-directional TAFT (1952) waves with a 25-second duration. Figure 5 shows the PGA-maximum node displacement relationship for the basic condition. Analysis revealed that for all three types of rise-span ratios, the limit states for insignificant and minor damage occurred around 0.2g and 0.4g, respectively. However, the limit states for moderate and severe appeared earlier with increasing rise-span ratios, primarily due to the varying stress characteristics of the structure under different rise-span ratios.

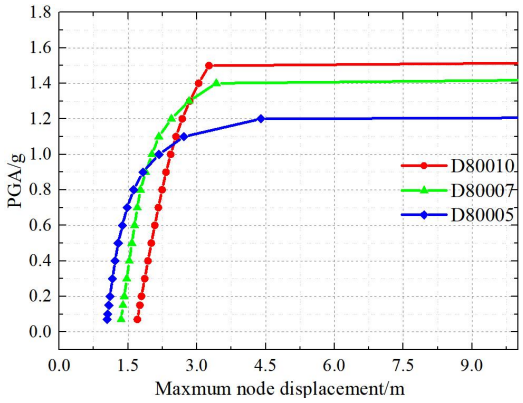

Figure 5: Response curves for the basic conditions of SSMS.

Using the D80005 structure as an example. LS1 and LS2 criteria are defined as the occurrence of 1P and 8P yielding members, respectively, as depicted in Figure 6. In the basic condition, 1P and 8P members appeared at 0.15g and 0.4g, respectively. With GFRP reinforcement, even at lower KF values, LS1 and LS2 critical load amplitudes increased by approximately 0.2g. At KF=80%, the increment amplitude exceeds 0.8g, with GFRP showing a particularly pronounced enhancement in LS1 critical load amplitude.

Comparing with the control group, when KF < 50%, as the thickness difference between the steel tube and the GFRP layer gradually decreases, the difference between GFRP group and control grop shows a trend of increasing first and then decreasing. When 50% < KF <60%, the GFRP group demonstrates

performance comparable to or slightly superior to the control group, notably surpassing the control group at higher KF values. Analyzing the maximum nodal displacement of the structure during occurrences of 1P and 8P members, it is evident that when KF < 60%, the reduction in displacement is relatively minor. However, as KF exceeds 60%, the reduction effect on critical displacement becomes increasingly pronounced. At KF=80%, the reduction rate exceeds 20%, which is significantly higher compared to the control group. GFRP reinforcement significantly improves the structure's ability to remain intact or incur only minor damage under seismic loads. Additionally, it reduces structural deformation, thus enhancing overall seismic performance.

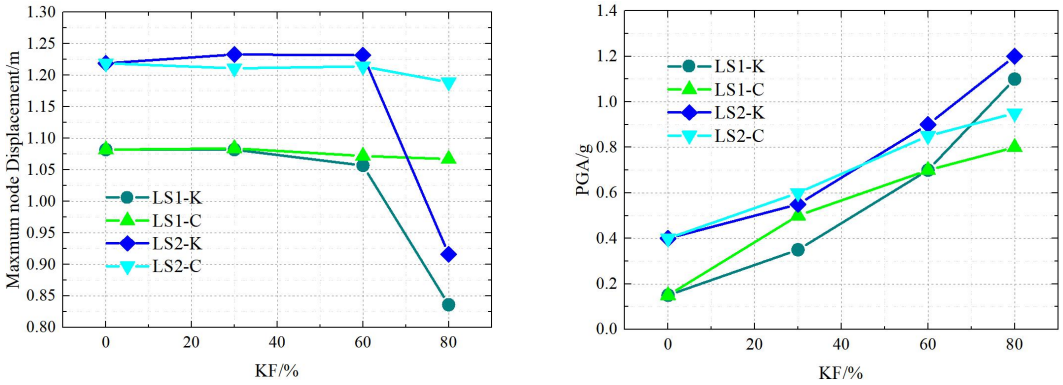

a) Maximum nodal displacement

b) Load amplitude

Figure 6: Response of LS1 and LS2

LS3 and LS4 are defined as the degradation of structural stiffness and structural collapse, respectively. It is found that with the increase of KF, the critical values of LS3 and LS4 have been significantly increased. Compared with the basic condition, at KF=60%, they increase by 1.1g and 2.1g respectively, which is basically the same as the control group, but it is significantly better than the control group when KF>60%. The plastic development situation is shown in Figure 7. Under LS3 conditions, the curve of the GFRP group is closer to the control group, and it also shows a trend of being better than the control group when KF>60%, indicating that GFRP can effectively improve the stiffness of the structure. Under LS4 conditions, the GFRP group is closer to the control group when KF<60%, and when KF=80%, the proportion of 1P and 8P members in the structure is about 30% higher than that of the control group, and the average plastic strain is about 4 times that of the control group. This indicates that using GFRP can effectively increase the range and depth of structural plastic development before collapse, so that the structure collapses only after withstanding larger deformations, thereby reducing casualties and economic losses caused by earthquakes.

4.3. Economic analysis

To facilitate a more intuitive comparison of the economic viability of GFRP-reinforced structures at varying KF values, structures comprised of different components were standardized with identical section libraries. Within the composite tube section library, component dimensions such as the equivalent outer diameter of steel tubes (D_{eq}), equivalent wall thickness (t_{eq}), and component density (ρ_{eq}) were utilized. Stability analysis of the structure was conducted based on full-span uniformly distributed loads,, confirming that the stability bearing capacity across different structures met the requisite double safety factor standard. Following market analysis, the cost of Q420 architectural round steel pipes was estimated at approximately 5500 yuan per ton, while S2 glass fiber/E51 epoxy resin stood at about 50000 yuan per ton. Taking into account corrosion prevention for architectural round steel pipes, a coating scheme with a 20-year lifespan was selected, priced at around 62 yuan per square meter. However, due to GFRP's excellent environmental resistance, structures fashioned from composite pipes forego the need for corrosion prevention measures. The cost and service life curve comparison of different structures, as depicted in Figure 8, illustrates that structures crafted from composite pipes (with volume rates of 30% and 60%) exhibit superior long-term economic feasibility when solely considering material prices, thus presenting a judicious choice for application in SSMS.

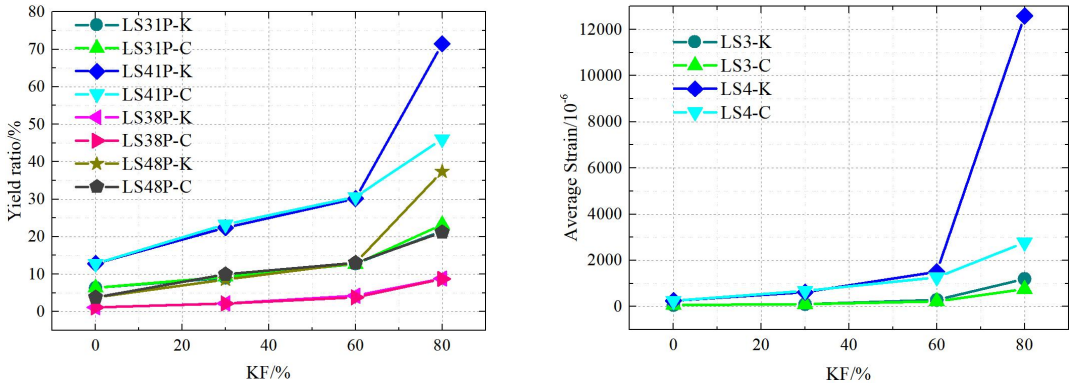

a) 1P and 8P members b) Average plastic strain

Figure 7: Response of LS3 and LS4

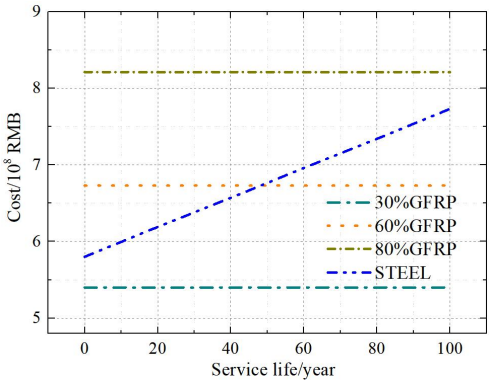

Figure8: Comparison of cost-lifespan curves for different structures

4. Conclusion

The three-dimensional grid dome-type SSMS, which meets the stability bearing capacity requirements with a safety factor of two, was reinforced using GFRP. A traditional building circular steel pipe structure with equal cross-section dimensions was employed as the control group. The study explored the enhancement effects of GFRP on the static and seismic performance of the SSMS, while also considering economic factors. The following conclusions were drawn:

In the static stability and performance analysis, the difference between the GFRP-reinforced structure and the control group decreased first and then increased as the disparity in thickness between the GFRP layer and the steel pipe grew. When this difference was significant, the synergy between materials suffered, leading to a peak discrepancy when KF was around 30%. However, when KF exceeded a critical value, typically around 60%, the GFRP group significantly outperformed the control, increasing the safety factor by up to 300% and reducing peak stress and node displacement by 70%. This effect was more pronounced in structures with smaller rise-span ratios.

GFRP enhances the SSMS structure across four seismic Limit states. It can increase the critical load by up to 0.8g for insignificant or minor Limit states, reducing deformation and enhancing structural integrity probality under seismic loads. For stiffness degradation and collapse Limit states, GFRP extends the range and depth of plastic development in the structure before collapse, delaying collapse until the structure undergoes greater deformation, thus reducing post-earthquake casualties and losses. Compared to the control, similar trends were observed with static analysis, the critical KF values range of different limit states are between 40% and 60%.

The analysis of GFRP-reinforced structures with similar safety factors under different KF values suggests that structures composed of composite components (KF=30%~60%) exhibit better long-term

economic viability. Therefore, considering structural static stability, seismic performance, and economic factors together, GFRP reinforcement schemes with KF values ranging from 50% to 60% can be considered a reasonable choice for SMSS.

References

[1] Z. S. Makowski, "Space structures of today and tomorrow," *In: Proceedings of third international conference on space structures,* pp. 1–8, 1984.

[2] A. ElSheikh, "Development of a new space truss system," *J Constr Steel Res,* vol. 37, no. 3, pp. 205-227, 1996.

[3] A. M. M. Kawaguchi, I. Tatemichi, "Design, tests and realization of `suspendome' system," *Journal of the International Association for Shell & Spatial Structures,* pp. 179–192, 1999.

[4] W. J. Kang, Z. H. Chen, H. F. Lam, and C. R. Zuo, "Analysis and design of the general and outmost-ring stiffened suspen-dome structures," *Eng Struct,* vol. 25, pp. 1685-1695, 2003.

[5] H. J. Wang, F. Fan, H. L. Qian, X. D. Zhi, and E. C. Zhu, "Full-Process Analysis of Pretensioning Construction of Dalian Gym," *Adv Mater Res-Switz,* vol. 163-167, pp. 200-204, 2011.

[6] Y. J. He, X. H. Zhou, and X. T. Zhang, "Finite element analysis of the elastic static properties and stability of pretensioned cylindrical reticulated mega-structures," *Thin Wall Struct,* vol. 60, pp. 1-11, 2012.

[7] Q. W. Zhang, Y. Zhang, L. Yao, F. Fan, and S. Z. Shen, "Finite element analysis of the static properties and stability of a 800 m Kiewitt type mega-latticed structure," *J Constr Steel Res,* vol. 137, pp. 201-210, 2017.

[8] Z. B. Zhao and Y. Zhang, "Seismic Performance Comparison of Three-Type 800 m Spherical Mega-Latticed Structure City Domes," *Sustainability-Basel,* vol. 15, no. 9, 2023.

[9] Q. W. Zhang, Z. B. Zhao, J. F. Chen, F. Fan, and S. Z. Shen, "On the static properties and stability of 800 m long-span mega-latticed suspension structures," *Structures,* pp. 139-151, 2020.

[10] Y. L. K. Tan, Y. Zhang, Q. W. Zhang, and F. Fan, "Static properties and stability of super-long span aluminum alloy mega-latticed structures," *Structures,* vol. 33, pp. 3173-3187, 2021.

[11] Y. L. K. Tan, Y. Zhang, Q. W. Zhang, and F. Fan, "Structural performance of a novel combined nested bolted joint for aluminum alloy mega-latticed structures," *Structures,* vol. 57, 2023.

[12] J. J. Zeng, Y. Y. Ye, W. T. Liu, Y. Zhuge, Y. Liu, and Q. R. Yue, "Behaviour of FRP spiral-confined concrete and contribution of FRP longitudinal bars in FRP-RC columns under axial compression," *Eng Struct,* vol. 281, 15 2023.

[13] M. Orouji and E. Najaf, "Effect of GFRP rebars and polypropylene fibers on flexural strength in high-performance concrete beams with glass powder and microsilica," *Case Stud Constr Mat,* vol. 18, 2023.

[14] H. El-Kady, O. Amer, A. H. Ali, and H. Haggag, "Experimental Investigation on the Cyclic In-Plane Behavior of GFRP-Reinforced Concrete Shear Walls," *Buildings-Basel,* vol. 12, 2022.

[15] Q. J. Wu and X. D. Zhi, "Experimental and numerical study of GFRP-reinforced circular steel tube under axial compression," *J Constr Steel Res,* vol. 168, 2020.

[16] P. Feng, L. L. Hu, P. Qian, and L. P. Ye, "Compressive bearing capacity of CFRP-aluminum alloy hybrid tubes," *Compos Struct,* vol. 140, pp. 749-757, 2016.

[17] Q. W. Zhang, Y. An, Z. B. Zhao, F. Fan, and S. Z. Shen, "Model selection for super-long span mega-latticed structures," *J Constr Steel Res,* vol. 154, pp. 1-13, 2019.

[18] Q. Wu, "Research on axial compression and low-velocity impact performance for the circular constructional steel tube wound by gfrp," (in Chinese), Harbin Institute of Technology, 2019.